Increased field-emission site density from regrown carbon nanotube films

Cite as: J. Appl. Phys. **97**, 104309 (2005); https://doi.org/10.1063/1.1897836
Submitted: 01 July 2004 • Accepted: 08 March 2005 • Published Online: 03 May 2005

Y. Y. Wang, S. Gupta, M. Liang, et al.

Increased field-emission site density from regrown carbon nanotube films

Y. Y. Wang, S. Gupta, M. Liang, and R. J. Nemanich[a)]
Department of Physics, North Carolina State University, Raleigh, North Carolina 27695-8202

(Received 1 July 2004; accepted 8 March 2005; published online 3 May 2005)

Electron field-emission properties of as-grown, etched, and regrown carbon nanotube thin films were investigated. The aligned carbon nanotube films were deposited by the microwave plasma-assisted chemical vapor deposition technique. The surface of the as-grown film contained a carbon nanotube mat of amorphous carbon and entangled nanotubes with some tubes protruding from the surface. Hydrogen plasma etching resulted in the removal of the surface layer, and regrowth on the etched surface displayed the formation of a new carbon nanotube mat. The emission site density and the current–voltage dependence of the field emission from all of the samples were analyzed. The results showed that the as-grown sample had a few strong emission spots and a relatively high emission current density ($\sim 20\ \mu A/cm^2$ at $1\ V/\mu m$), while the regrown sample exhibited a significantly increased emission site density. © *2005 American Institute of Physics*. [DOI: 10.1063/1.1897836]

I. INTRODUCTION

Carbon nanotubes (CNTs) have attracted a great deal of attention both from the fundamental and technological standpoints due to their unique structural, chemical, electronic, and mechanical properties.[1] Different methods have been developed and employed to synthesize carbon nanotubes.[1] Chemical vapor deposition (CVD) is one of the most commonly used techniques because it enables carbon nanotubes to grow directly on the substrates, which may facilitate the fabrication of carbon nanotube-based devices such as field-effect transistors,[2] sensors,[3] and vacuum microelectronics.[4]

Electron field emission from carbon nanotubes (both multi- and single-walled) has become an important area of research.[5] This is because carbon nanotube emitters are able to deliver a relatively high emission current or current density, show an extremely low applied threshold field, and have demonstrated emission operation of more than 5000 h.[5,6] In addition, they also show excellent chemical stability.[7,8]

For most field-emission devices, a low turn-on field (<1–$5\ V/\mu m$), a large current density (50–$100\ \mu A/cm^2$), and a high stability (or long lifetime) are required.[5] While for the field-emission arrays (FEAs), the uniformity of the emission is also a crucial parameter. Several groups have reported an increase in the emission site density (ESD) of carbon nanotubes-based field emitters by optimizing their array densities (reducing electrostatic screening effects),[9] by focused ion and laser irradiation (increasing the defect density),[10] and by exposure to hydrogen gas (removing catalyst particles on the surface).[11] Interestingly, the measurements reveal the actual ESD of $\sim 10^4/cm^2$ compared to the nanotube areal density which is $>10^8/cm^2$.[12] It is still an open question as to why such a small proportion of nanotube emitters participate in the field-emission properties. We are also left to question whether these emitters are representative of the overall population or whether they are special cases. In order to explore these issues, we elucidated that through hydrogen plasma etching followed by a regrowth process, the electron emission site density from carbon nanotube films were significantly affected. Our results indicate that the emitters that contribute to the emission current in relatively large area measurements represent only a small fraction of the CNTs, which may be described as special or long-protruded carbon nanotubes.

II. EXPERIMENTAL DETAILS

The carbon nanotube samples employed in the present study are labeled as as-grown, etched, and regrown. All of the samples were grown and processed in a microwave plasma-assisted CVD reactor (MPCVD),[13] which is also used to grow poly- and nanocrystalline diamond films.[14] The catalyst used was iron with a thickness of 80 nm deposited by dc magnetron sputtering on commercial Si(100) wafers. The as-grown sample was deposited for 30 min using ammonia (NH_3) and acetylene (C_2H_2) in a 4:1 ratio. The substrate temperature was maintained at 900 °C, and the chamber pressure and plasma power were kept constant at 20 Torr and 600 W, respectively. The etched sample was first grown for 30 min using the same conditions as for the as-grown sample. Then the C_2H_2 and NH_3 were shutoff and hydrogen (H_2) with a flow rate of 200 SCCM (SCCM denotes cubic centimeter per minute at STP) was immediately introduced into the chamber. Plasma etching was performed for 10 min at a substrate temperature of 800 °C. The regrown sample was deposited on the etched surface by employing the same growth conditions for a period of 15 min. The process is carried out by cutting off the hydrogen flow and admitting the NH_3 and C_2H_2 gas feedstocks into the chamber. For the etched and regrown samples, each stage of the processing was carried out immediately following the previous stage with no significant time delay. The growth parameters and surface treatment steps are listed in Table I.

All of the samples ($2\times 1\ cm^2$) were characterized by scanning electron microscopy (SEM, Model JEOL 6400F). The field-emission characterization system used here em-

a)Electronic mail: robert_nemanich@ncsu.edu

TABLE I. The growth parameters and surface treatment steps for the as-grown, etched, and regrown samples.

Process parameters	Growth	Etching	Regrowth
Gas feedstocks	NH_3/C_2H_2	H_2	NH_3/C_2H_2
Pressure (Torr)	20	20	20
Microwave power (W)	600	600	600
Flow rate (SCCM)	70/18	200	70/18
Substrate temperature (°C)	900	800	900
Time (min)	30	10	15
Surface treatment	Growth	Etching	Regrowth
As-grown	X[a]		
Etched	X	X	
Regrown	X	X	X

[a]X implies the treatment has taken place.

ploys parallel plate or diode geometry (cathode–anode) and is equipped with a phosphor-coated indium tin oxide (ITO) screen which acts as an anode and enables observation of the field-emission sites. The interelectrode (the anode and sample) distance (d) was kept fixed at ~0.8 mm during all measurements. A Keithley 237 source measuring unit was used to measure the I–V curves during emission imaging. The chamber pressure in this system during the emission measurements was $\sim 4\times 10^{-7}$ Torr.

III. RESULTS

A. As-grown carbon nanotube film

A cross-sectional SEM image of the as-grown CNT film is shown in Fig. 1(a). The film thickness is ~50 μm, which was obtained in 30 min yielding an average growth rate of 1.6 μm/min. Figure 1(b) is a magnified image of the part of the film beneath the top surface exhibiting that multiwall carbon nanotubes (MWNT) grow largely perpendicular to the substrate, and tend to entwine together. Figure 1(c) presents an image of the structures near the film surface. The surface is covered by a CNT mat with a thickness of 5–7 μm. Some of the tubes (indicated by the arrows) protrude out of the surface of the films. They have an average diameter of ~60 nm and are longer by approximately 10 μm than those at the surface. A magnified view [see Fig. 1(d)] of the carbon nanotube mat seems to indicate that the nucleation to grow carbon nanotubes evidently takes place at the film surface as discussed in detail below.

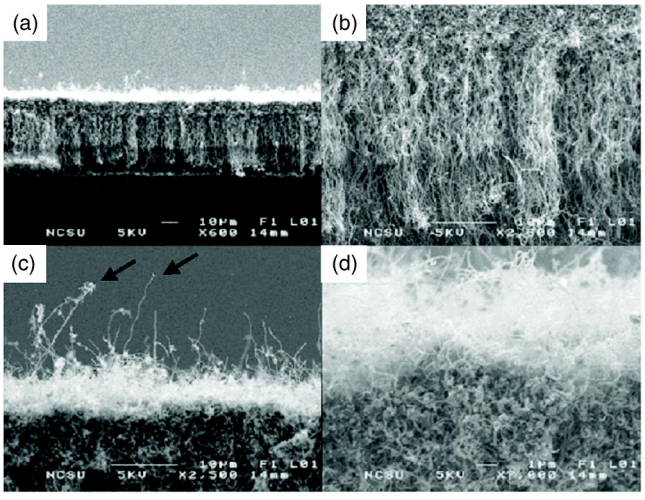

FIG. 1. (Color online) Scanning electron micrographs of as-grown carbon nanotube film at different magnifications revealing the morphology (a) at 600×, (b) just beneath the top surface at 2300×, (c) structures at the film surface at 2500×, and (d) carbon nanotube mat at 7000×.

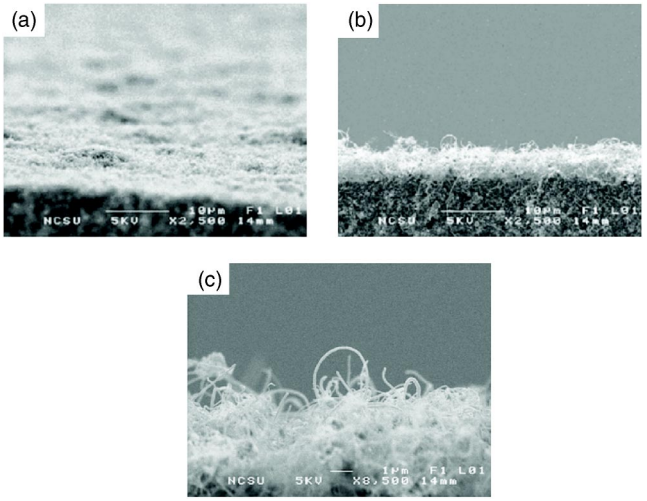

FIG. 2. (Color online) Scanning electron micrograph of the surface of the etched sample (a), and the regrown sample at ×2300 (b), and ×8500 (c).

B. Etched and regrown carbon nanotube film

The hydrogen plasma cleaning was performed for 10 min on the as-grown sample. Compared to the as-grown sample surface [Fig. 1(c)], the micrograph of the hydrogen plasma-etched sample surface shown in Fig. 2(a) does not display a CNT mat and the associated protruding tubes. The mechanism of the etching process typically involves both physical ion bombardment and chemical reaction, where the latter involves a sequence of several hydrogenation steps:[15]

$$\text{(graphite)} - \text{C} + \text{H} \rightarrow \text{(graphite)} - \text{C} - \text{H},$$

$$\text{(graphite)} - \text{CH} + \text{H} \rightarrow \text{(graphite)} - \text{CH}_2, \ldots, \quad (1)$$

with volatile hydrocarbon species or radicals as the products which are released at the relatively high process temperatures employed in the deposition. Since CNTs are primarily sp^2-bonded carbon (sp^2 C), the chemical reactivity in this process is determined by the interaction of sp^2 C and atomic hydrogen. This process is also considered to be important in the deposition of diamond films.[15] By adopting this approach, we attempted to obtain a clean, planarized surface of aligned multiwall carbon nanotubes.

To study if there are any catalyst particles at the surface which assist the growth of CNTs, x-ray photoelectron spectroscopy (XPS) was used for surface chemical analysis. Both the as-grown and etched samples show a strong C_{1S} peak at 284.5 eV, but no evidence of the Fe_{2P} peaks which appear between 700 and 730 eV, indicating almost no Fe at the surface of the CNT mat. In order to check if the carbon nanotubes regrow on the etched surface, we used the same

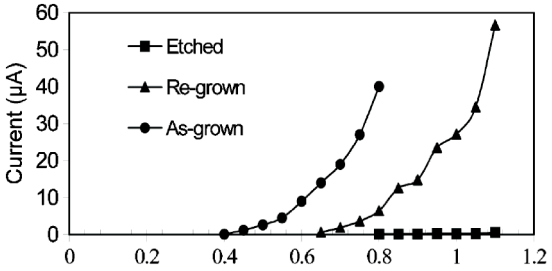

FIG. 3. Emission current vs voltage curves for the as-grown, etched, and regrown samples.

growth conditions employed previously. The surface of the regrown sample is shown in the SEM image [see Fig. 2(b)], which exhibits an ~6–7-μm-thick layer of CNT mat similar to the as-grown sample but without the protruding tubes. Evidence for the "regrown" carbon structures to be nanotubes is clearly displayed in Fig. 2(c), which is a high-resolution scanning electron micrograph of the regrown surface, where the nanotubes appear randomly aligned and show a similar height without long protruding CNT.

C. Field-emission measurements

Electron field-emission measurements were performed on each of the samples. For the *I–V* (emission current versus applied voltage) curves, a voltage sweep from 0 to −1100 V with an increment of −50 V was applied to the sample. Images of the spatial distribution of emission sites were recorded by a digital camera. Figure 3 shows representative *I–V* characteristics for all of the samples studied. For an emission current of 1 μA, the applied voltage is approximately 450 V for the as-grown sample and 700 V for the regrown sample. The emission current of the etched sample is <1 μA at an applied voltage of 1100 V. At any applied voltage, the as-grown sample shows the highest emission current, while the etched sample has the lowest. For example, at a voltage of 800 V, the emission current (or emission current density) for the as-grown, etched, and regrown samples is 40, 0.09, and 6.4 μA (or 20, 0.045, and 3.2 μA/cm^2), respectively.

Figures 4(a)–4(h) display the images of the phosphor screen which indicates the emission sites from the samples (as-grown, etched and regrown) at applied voltages of 700, 800, and 1000 V. We observe that the field emission from the as-grown sample [Figs. 4(a) and 4(b)] is relatively nonuniform, and there are several quite strong emission spots. As the applied voltage increases from 700 to 800 V, the emission current from these spots increases while only a few new emission sites are observed. To protect the phosphor screen from being damaged or excessively sputtered, the voltage was limited to this value. The field-emission sites from the etched sample [see Figs. 4(c)–4(e) display a single isolated spot, which appears when the voltage is increased to 800 V. A few emission sites are detected when the voltage is increased further to 1000 V, but the emission current is still below 1 μA. In contrast, field emission from the regrown sample exhibits a relatively higher density of emission sites with more uniform emission characteristics [see Figs. 4(f)–4(h)]. As the applied voltage increases, new emission sites appeared each with approximately similar intensity. Compared to the as-grown sample, the emission current from the regrown sample is still lower, but it has many more emission sites with similar emission from each site.

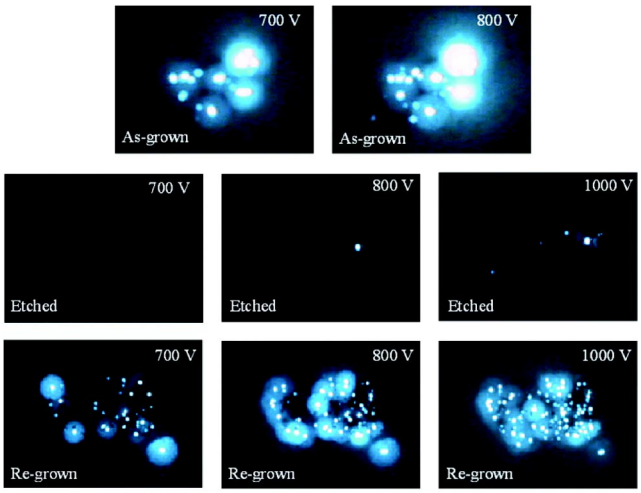

FIG. 4. (Color online) Field-emission images from (a)–(b) the as-grown, (c)–(e) etched, and (f)–(h) regrown samples at applied voltages of 700, 800, and 1000 V, respectively.

Figure 5 presents a Fowler–Nordheim (FN) plot of $\ln(1/V^2)$ vs $1/V$ for the *I–V* curves shown in Fig. 3. We note that since the field-emission test system does not allow an accurate measurement of the cathode–anode distance (d), we cannot estimate the exact values of β (the geometrical field enhancement factor), rather another parameter γ ($=\beta/d$) is introduced. Assuming a work function (ϕ) of ~5 eV, the γ can be derived from the slopes ($=-6.83\times10^7\phi^{1.5}\gamma$) of the FN plots. The γ values obtained for the as-grown and regrown samples were 2.36×10^5/cm and 1.08×10^5/cm, respectively. The corresponding local electric field ($F_{\mathrm{loc}}=\gamma^* V$) values deduced for the emission current of 1 μA from the as-grown and the regrown samples are 1.06×10^8 and 7.56×10^7 V/cm.

IV. DISCUSSION

Our results established that the relatively complex surface structures shown for the as-grown sample are influenced

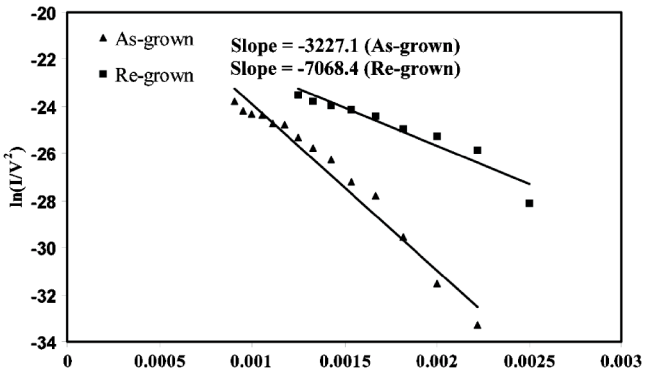

FIG. 5. Shown is FN plot [$\ln(I/V^2)$ vs I/V] for the as-grown and regrown samples.

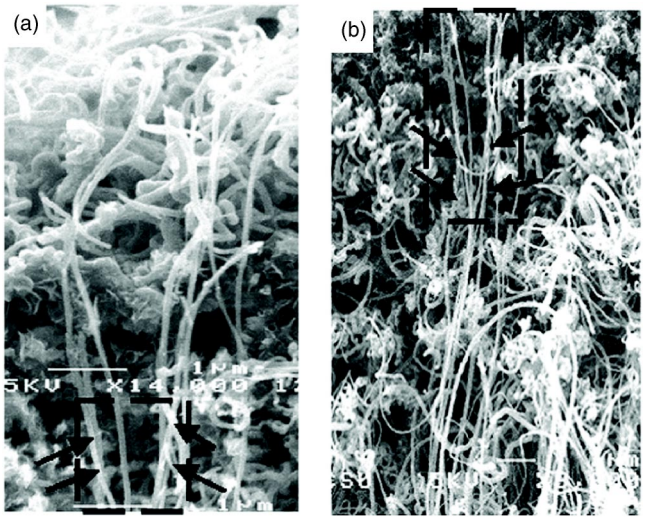

FIG. 6. (Color online) Scanning electron micrographs of the regrown nanotube mat tracing a few tubes, exhibiting that they originate from the bottom of the film: (a) top at 14 000× (b) bottom at 8000×. The dotted blocks show where the trace starts.

by the growth time. The experiments show that growth for shorter times (~15 min) has less surface structure compared to the longer times (~30 min) shown in Fig. 1(c), where a layer of CNT mat is formed at the surface. In our comparative study, surface treatments of hydrogen plasma etching and regrowth were performed in order to planarize the sample surface and to determine if the regrowth surface has improved characteristics in terms of uniformity and a reduction of undesired amorphous carbon (*a*-C). After the regrowth, a layer of CNT mat appeared on the etched surface but with improved uniformity [see Fig. 2(b)].

The new layer of carbon nanotube mat from the regrown sample is interesting as to where the CNT nucleate or originate. The CNTs of the mat appear to be confined at the film surface suggesting that they grow from the surface of the etched CNT films. But our XPS spectrum showed no clear evidence of iron catalyst at the surface of either the as-grown or etched samples. Alternatively, we consider whether this new layer might either represent continuous growth of the existing CNTs from the substrate or that growth is promoted from the surface of the CNT tips and/or surface *a*-C aggregation without transition-metal particle assistance to catalyze the growth of the nanotubes. In fact, Obraztsov *et al.*[16] suggested that multiwalled nanotubes can be grown on nanostructured graphite by either dc or thermal CVD plasma without the assistance of a metal catalyst. To address the origin of CNTs appearing at the regrown sample surface, we carried out more detailed SEM measurements and a representative example is shown in Fig. 6. In this sequence of images [from Figs. 6(a) and 6(b)] we traced a few tubes from the nanotube mat. The SEM images apparently show that these tubes (see arrows) originate from the catalyst layer at the bottom of the films.

We suggest that amorphous carbon (*a*-C) can significantly affect the film growth and result in different film-surface morphology. The *a*-C may form at the surface and/or at the space in between the nanotubes during the growth, which may block the carbon supply to the catalyst at the substrate and therefore, slow the growth of the nanotubes in the adjacent region. However, this effect is not expected to be uniform, and some nanotubes may grow relatively faster and tend to protrude out of the surface.

As shown in Fig. 2(c), it is apparent that the structure at the regrown film is primarily carbon nanotubes with little *a*-C. Possible reasons for the reduced *a*-C at the regrown sample surface include (i) hydrogen plasma etches the as-deposited *a*-C at the surface, which reduces the possibility of further *a*-C accumulation, (ii) during regrowth, *a*-C may form but the relatively shorter growth time may result in reduced *a*-C deposits compared to the longer growth time of the initial film growth.

The field-emission images show that the emission behavior is strongly influenced by different surface morphology. Comparing the surface morphology of the as-grown and regrown samples, the carbon nanotube mat has a similar areal density [see Figs. 1(c) and 2(b)]. The most notable difference is the protrusion of individual tubes at the as-grown film surface. Cumings *et al.* observed by electron holography that the electric field is concentrated precisely at the tips of the nanotubes.[17] Zheng *et al.* used quantum-mechanical simulations to show a result consistent with the experiment carried out by Cumings.[18] Therefore, for the as-grown sample a few intensive emission spots may correlate to those protruding tubes with the electric field localized at the tips. Nilsson *et al.* proposed that the β distribution has an exponential dependence for their carbon-based thin films.[19] Within this model, the electron emission is dominated by those emitters with high βs. A few strong emission spots from the as-grown sample indicate that the surface morphology of the as-grown sample induces a nonuniform β distribution, where sites with larger β dominate and lower β sites only deliver small amounts of current. Moreover, a high density of similar height nanotubes will lead to field screening. The adjacent CNTs will limit the field enhancement below that expected for a single nanotube, and the high-density regions will display a lower-field enhancement.[9]

For our regrown sample a higher density of emission sites with similar emission intensities was obtained. This observation suggests that the regrown nanotubes of similar protruding heights may induce a more uniform distribution of β. However, the β of the emitting sites may be relatively lower compared to the as-grown film where those individual protruding nanotubes may exhibit substantially increased β. Therefore, the regrown films show a relatively lower current density even though they have more emission sites.

Since electron field emission is also a surface sensitive phenomenon,[20] considering the working pressure of $\sim 4E-10^{-7}$ Torr in our study, the role of adsorbates and other surface interactions is certainly not ruled out in affecting the field-emission properties. The reason that more new emission sites with similar emission from each site shown in Figs. 4(f)–4(h), which were otherwise dormant at lower voltages, tend to become activated at relatively higher applied voltages may likely be attributed to the adsorption-desorption process. In addition, Collazo *et al.*[21] reported an increased emission current which has been attributed to the presence of adsor-

bates on the nanotubes and explained that the adsorbates would introduce a resonant state enhancing the tunneling probability of the electrons.

V. CONCLUSIONS

In summary, aligned multiwalled carbon nanotube films were deposited, processed, and regrown by the microwave plasma-assisted CVD technique. It was found that the as-grown sample had a relatively higher emission current, a lower turn-on field, and a few strong emission sites. The regrown sample showed more uniform field emission and a significant increase in the emission site density with a moderate emission current and a low turn-on field. The different field-emission properties of the as-grown film and the regrown film are ascribed to the surface morphology and the structure of the film. In this study, we have introduced two postdeposition processes including hydrogen plasma etching and MPCVD regrowth. Through optimizing these two processes and the CNT growth, it may be possible to control the effects of screening to significantly increase the emission site density of carbon nanotube films.

ACKNOWLEDGMENTS

We acknowledge Dr. R. Collazo (Department of Materials Science and Engineering, NC State University) for his fruitful suggestions in this work. This research is supported in part by the TEC ONR-MURI and the DOE-CESP center at Argonne National Laboratory.

[1]H. Dai, Surf. Sci. **500**, 218 (2002).
[2]K. Xiao, Y. Liu, P. Hu, G. Yu, X. Wang, and D. Zhu, Appl. Phys. Lett. **83**, 150(2003).
[3]S. Ghosh, A. K. Sood, and N. Kumar, Science **299**, 1042 (2003).
[4]J. Kwo, M. Yokoyama, C. Lee, F. Chuang, and I. Lin, J. Vac. Sci. Technol. B **19**, 1023 (2001).
[5]J. M. Bonard, K. A. Dean, B. F. Coll, and C. Klinke, Phys. Rev. Lett. **89**, 197602-1 (2002).
[6]S. Uemura, J. Yotani, T. Nagasako, H. Kurachi, H. Yamada, T. Ezaki, T. Maesoba, T. Nakao, M. Ito, Y. Saito, Y. Ando, X. L. Zhao, and M. Yumura, *Light Sources 2004*, Institute of Physics Conference Series, Vol. 182, p. 125 (2004).
[7]W. Zhu, C. Bower, G. P. Kochanski, and S. Jin, Solid-State Electron. **45**, 921 (2001).
[8]W. A. de Heer, A. Chatelain, and D. Ugarte, Science **270**, 1179 (1995).
[9]L. Nilsson *et al.*, Appl. Phys. Lett. **76**, 2071 (2000).
[10]A. Sawada, M. Iriguchi, W. J. Zhao, C. Ochiai, and M. Takai, J. Vac. Sci. Technol. B **21**, 362 (2003).
[11]S. C. Lim *et al.*, J. Vac. Sci. Technol. A **19**, 1786 (2001).
[12]O. Groning, O. M. Kuttel, Ch. Emmenegger, P. Groning, and L. Schlapbach, J. Vac. Sci. Technol. B **18**, 665 (2000).
[13]Y. Y. Wang, G. Y. Tang, F. A. M. Koeck, J. M. Garguilo, B. Brown, and R. J. Nemanich, Diamond Relat. Mater. **13**, 1287 (2004).
[14]F. A. M. Koeck, J. M. Garguilo, and R. J. Nemanich, Diamond Relat. Mater. **10**, 1714 (2001).
[15]J. Kuppers, Surf. Sci. Rep. **22**, 249 (1995).
[16]A. N. Obraztsov, A. P. Volkov, K. S. Nagovitsyn, K. Nishimura, K. Morisawa, Y. Nakano, and A. Hiraki, J. Phys. D **35**, 357 (2002).
[17]J. Cumings, A. Zettl, M. R. McCartney, and J. C. H. Spence, Phys. Rev. Lett. **88**, 056804 (2002).
[18]X. Zheng, G. H. Chen, Z. Li, S. Deng, and N. Xu, Phys. Rev. Lett. **92**, 106803 (2004).
[19]L. Nilsson, O. Groening, P. Groening, O. Kuettel, and L. Schlapbach, J. Appl. Phys. **90**, 768 (2001).
[20]S. H. Jo, Y. Tu, Z. P. Huang, D. L. Carnahan, J. Y. Huang, D. Z. Wang, and Z. F. Ren, Appl. Phys. Lett. **84**, 413 (2004).
[21]R. Collazo, R. Schlesser, and Z. Sitar, Appl. Phys. Lett. **78**, 2058 (2001).